Influence of Anatomical Detail and Tissue Conductivity Variations in Simulations of Multi-Contact Nerve Cuff Recordings

Article *in* IEEE Transactions on Neural Systems and Rehabilitation Engineering · November 2016

DOI: 10.1109/TNSRE.2016.2633005

5 authors, including:

Purbasha Garai
University of Toronto

Martin Schuettler
CorTec GmbH, Freiburg, Germany

Thomas Stieglitz
University of Freiburg

José Zariffa
Toronto Rehabilitation Institute - University Health Network

Garai, P., Koh, R. G., Schuettler, M., Stieglitz, T., & Zariffa, J. (2017). Influence of anatomical detail and tissue conductivity variations in simulations of multi-contact nerve cuff recordings. IEEE Transactions on Neural Systems and Rehabilitation Engineering, 25(9), 1653-1662
Author's accepted version. The final publication is available at https://ieeexplore.ieee.org

Influence of anatomical detail and tissue conductivity variations in simulations of multi-contact nerve cuff recordings

Purbasha Garai, Ryan G.L. Koh, *Student Member, IEEE*, Martin Schuettler, *Member, IEEE*, Thomas Stieglitz, *Senior Member, IEEE*, and José Zariffa, *Member, IEEE*

***Abstract*— Accurate simulations of peripheral nerve recordings are needed to develop improved neuroprostheses. Previous models of peripheral nerves contained simplifications whose effects have not been investigated. We created a novel detailed finite element (FE) model of a peripheral nerve, and used it to carry out a sensitivity analysis of several model parameters. To construct the model, *in vivo* recordings were obtained in a rat sciatic nerve using an 8-channel nerve cuff electrode, after which the nerve was imaged using magnetic resonance imaging (MRI). The FE model was constructed based on the MRI data, and included progressive branching of the fascicles. Neural pathways were defined in the model for the tibial, peroneal and sural fascicles. The locations of these pathways were selected so as to maximize the correlations between the simulated and *in vivo* recordings. The sensitivity analysis showed that varying the conductivities of neural tissues had little influence on the ability of the model to reproduce the recording patterns obtained experimentally. On the other hand, the increased anatomical detail did substantially alter the recording patterns observed, demonstrating that incorporating fascicular branching is an important consideration in models of nerve cuff recordings. The model used in this study constitutes an improved simulation tool and can be used in the design of neural interfaces.**

Index Terms—Finite element modeling; peripheral nerve interfaces; nerve cuff recordings; nerve imaging.

I. Introduction

Spinal cord injury (SCI) can result in permanent neurological damage and loss of sensorimotor function below the level of injury. Implanted systems for functional electrical stimulation (FES) can be used to restore some movement by causing paralyzed muscles to contract in a functional pattern [1]. While current implanted FES systems predominantly use pre-defined patterns of stimulation, the quality and robustness of the movements could be improved if appropriate feedback signals could be extracted and used to implement closed-loop control strategies. The sensory signals in peripheral nerves may be useful as feedback signals for the FES systems, if they could be reliably and selectively extracted. Various peripheral nerve interfaces have been proposed to record neural signals [2, 3]. Of these, cuff electrodes are appealing because they do not penetrate the nerve or damage the neural structures, and have been shown to be suitable for long-term recording [4-8]. On the other hand, since they are extraneural, cuff electrodes tend to lack selectivity and have lower signal-to-noise ratios (SNR) in comparison to penetrating electrodes.

Improving the selectivity of nerve cuff recordings requires novel multi-contact designs and tailored signal processing approaches, and has been the focus of several previous studies [9-15]. Accurate computer simulations of nerve cuff recordings are an essential part of this design process. A number of finite element (FE) models of peripheral nerves have been reported in the literature for this purpose [16-20]. However, all of these models had certain simplifications in common. First, the geometry of previous models was based on one cross section of the nerve (or a simplified cylindrical geometry) and was uniform in the longitudinal direction. Therefore, they lacked anatomical detail reflecting the progressive branching of the fascicles. Previous work has shown that longitudinal variations may be important in the context of selective nerve cuff recordings [21]. Detailed reconstruction of peripheral nerves is tedious [22] but important to verify models and be able to predict differences in simulation output compared to *in vivo* verifications. Second, the conductivity values used for the neural tissues in previous models have not been well validated. The values used in the models cited above can be traced back to studies that were not conducted in mammalian peripheral nerves, and their applicability in this context has been assumed but not confirmed. Specifically, the conductivity values used for the endoneurium are usually based on measurements from a study in the cat spinal dorsal column [23]. The perineurium values are based on measurements from a study in the frog sciatic nerve [24]. Epineurium conductivity has not been directly measured and was assumed to be equivalent to the transverse conductivity of the endoneurium.

Our objective in this study was to evaluate the impact on these model simplifications (anatomical detail and tissue conductivity values) on simulations of multi-contact nerve

Manuscript received June 16, 2016; revised October 7, 2016; accepted November 17, 2016. This work was supported in part by the Natural Sciences and Engineering Research Council of Canada (RGPIN-2014-05498).

P. Garai (purbasha.garai@mail.utoronto.ca), R.G.L. Koh (ryan.koh@mail.utoronto.ca) and J. Zariffa (jose.zariffa@utoronto.ca) are with the Toronto Rehabilitation Institute - University Health Network, Toronto, ON, M5G 2A2, Canada and the Institute of Biomaterials and Biomedical Engineering (IBBME), University of Toronto, Toronto, ON, M5S 3G9, Canada.

M. Schuettler (mschuettler@cortec-neuro.com) is with CorTec GmbH, Freiburg, Germany. T. Stieglitz (stieglitz@imtek.de) is with BrainLinks-BrainTools & the Laboratory for Biomedical Microtechnology, Department of Microsystems Engineering-IMTEK, University of Freiburg, Freiburg, Germany.

cuff recordings, using an anatomically accurate and experimentally validated FE model.

II. METHODS

The major steps of our study are as follows. We first collected the experimental data on which the model was based. We next constructed an FE model of the nerve. A sensitivity analysis was then conducted focused on determining the impact of tissue conductivity values on the simulation results. Lastly, the model parameters were finalized, and our anatomically detailed model was compared to a simplified model to ascertain the impact of the added detail on the results.

A. Experimental procedures

Acute experiments were performed on 14 Long-Evans rats (retired breeders) under isoflurane anesthesia. Neural activity was recorded from the sciatic nerve using a spiral polyimide nerve cuff electrode with two ring shape anodes and 8 cathodes in between distributed over the perimeter of the cuff [25] to establish tripolar electrode arrangements. The cuff had a total length of 22 mm and a diameter of 1 mm (Fig. 1). A needle electrode was inserted in the back of the animal to serve as a reference, and a quasi-tripolar arrangement was used (i.e., the monopolar measurements from the contacts in the middle ring were referenced to the average of the measurements from the two outer anodes). Data was acquired with a sampling frequency of 30 kHz and bandpass filtered between 250 Hz and 7.5 kHz, using a neural data acquisition system (Cerebus, Blackrock Microsystems, USA).

Afferent activity was evoked in each of the tibial, peroneal and sural fascicles in turn using mechanical stimuli. The foot was held by the claws, and the ankle was manually dorsiflexed and plantarflexed by approximately 60° to evoke proprioceptive activity in the tibial and peroneal branches, respectively [26]. A cutaneous stimulus to the heel using a Von Frey monofilament (300 g) was used to elicit activity in the sural branch [27]. 75 to 100 trials were performed for each stimulus. In off-line processing, periods when a stimulus was being applied were extracted from the recordings based on timing determined by finding peaks in a rectified-bin-integrated version of the signal, using 100ms windows. Then, action potentials (APs) for each type of stimulus were extracted from the identified periods using a manually selected threshold, aligned based on their positive peak, and averaged to obtain an average waveform for each stimulus and each recording contact in the cuff.

Once the sensory signals were recorded, the animal was euthanized and the nerve was harvested and imaged using magnetic resonance imaging (MRI). The nerve specimen was placed in formalin doped with 2 mM Gd-DTPA within a eppendorf tube for at least 48 hours prior to scanning. MRI was performed using a 7 Tesla Bruker Biospec 70/30 system, equipped with a BGS-12 gradient coil, 7.2 cm inner diameter linearly polarized RF transmit coil, and 4 coil phased array receiver coil. The full length of the nerve specimen was imaged with a 3D T1-weighted RARE technique, providing 30 x 30 x 250 µm³ spatial resolution over a 4.8x4.8x35 mm³ volume.

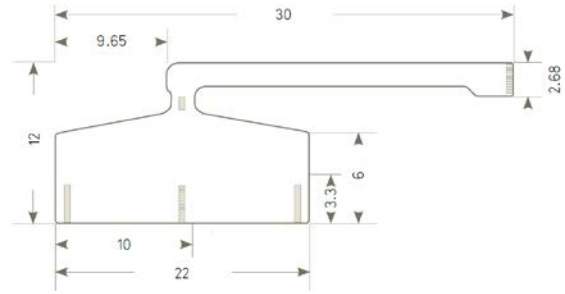

Fig.1. Schematic of the spiral nerve cuff used in this study. Dimensions are in mm. The 8 cathodal contacts have dimensions of 0.5×0.25 mm², with a gap of 0.15 mm between contacts.

The experimental procedures were approved by the Animal Care Committee of the University of Toronto.

B. Construction of the FE model

Once the neural recordings and imaging were completed, we selected one dataset as the basis for the model construction. The dataset chosen provided the best combination of neural signal and image quality.

1) Image preprocessing

The stack of nerve cross section images first needed to be aligned, due to some curvature in the nerve during fixation. A template matching plugin was used in ImageJ [28] using the normalized correlation coefficient method for stack alignment.

2) Segmentation

The aligned nerve cross sections were imported into Seg3D [29], a segmentation software, to trace the regions of interest. From the MRI scan of nerve cross sections, the fascicles and the epineurium were traced manually. The perineurium was then added with a minimum thickness of 0.065 mm around each fascicle. We had to maintain this thickness for finite element modelling, because thinner layers caused errors in the meshing process. After adding layers for each tissue type within the nerve, we further added a region to denote the cuff electrode with a thickness of 0.03 mm and diameter of 1.66 mm around the nerve. The distance between the contact rings was 10 mm. For simplicity, the outer rings of the cuff were

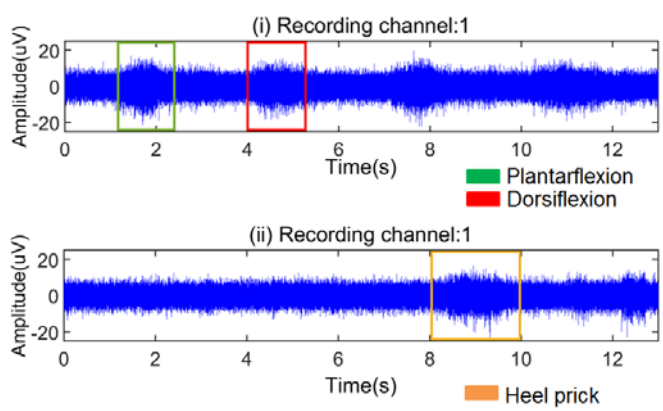

Fig. 2. Recordings obtained from one of the eight channels of the nerve cuff for (i) plantar flexion and dorsiflexion (ii) heel prick.

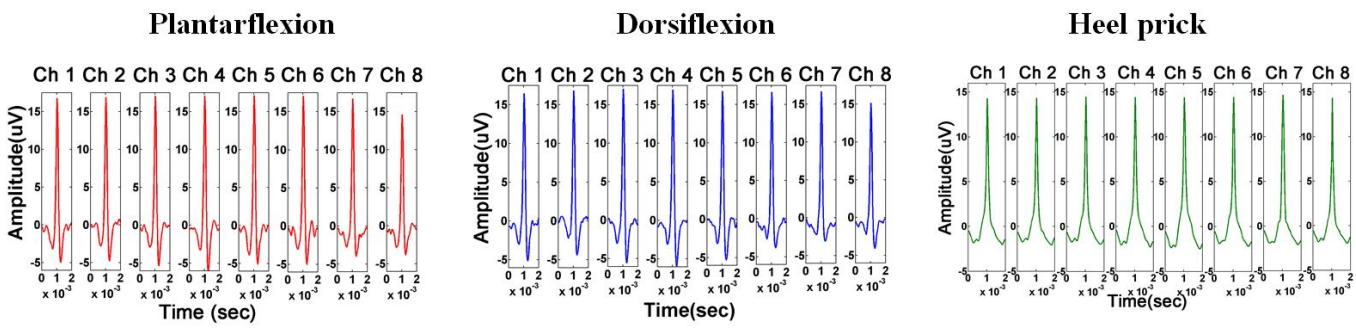

Fig. 3. Average waveform for (i) plantarflexion; (ii) dorsiflexion and (iii) heel prick on the different channels of a cuff electrode.

modeled as rings of multiple contacts similar to the middle ring (Figure 1), and the simulated recordings from all contacts in the outer rings were averaged at the leadfield generation stage (see Section II.B.4). The region in between the nerve and cuff was filled with saline. The saline layer had a radius of 0.17±0.12 mm around the whole nerve. Lastly, a saline layer was placed around the cuff, with a radius of 1.51 mm. The layers created for the regions were then exported to MATLAB where the volumetric image dataset was meshed.

3) Volumetric mesh generation

Iso2mesh, an open source MATLAB-based mesh generation and processing toolbox, was used to create a 3D tetrahedral FE mesh from the volumetric images [30]. A surface mesh was first generated from the grayscale image. A Laplacian smoothing algorithm was then applied to move the coordinates of the vertices of the mesh to smoothen irregularities in the mesh model. This process was applied iteratively 500 times to obtain the final smooth surface mesh. Once the surface meshes had been finalized for the boundaries between the different components of the model, a tetrahedral volumetric mesh was created from the surface meshes. A finer mesh was used for the inside of the nerve regions, while coarser mesh elements were used in the outer saline, where the geometry was simpler. The quality of the tetrahedral mesh was then evaluated by checking how close each element was to an equilateral tetrahedron, using the 'meshquality' function within the Iso2Mesh toolbox.

4) Construction of the leadfield matrix

We wish to use the FE model to predict how a source at a given location will affect the measurements at the cuff contacts. The information is encoded in a MxN leadfield matrix, **L**, whose entry (i,j) represents the influence of a unit current dipole at mesh element j on the potential recorded at electrode contact i. M is the number of electrode contacts, and N is the number of elements forming the tetrahedral mesh.

To construct **L**, we followed the process described by Weinstein *et al*. [31], using the SCIRun software package [32]. In the leadfield computed with the method described in [31], all values are referenced to one electrode used as the ground. Before any further analysis, the leadfield was converted to a tripolar reference by using the average of all contacts in the outer rings as the reference.

The default conductivity values for the leadfield computations were $8.26\text{x}10^{-2}$ S/m for the transverse direction of the endoneurium, 0.571 S/m for the longitudinal direction of the endoneurium, $2.1\text{x}10^{-3}$ S/m for the perineurium, and $8.26\text{x}10^{-2}$ S/m for the epineurium. 2 S/m was used for the saline and $1\text{x}10^{-7}$ S/m for the cuff [12, 19].

C. Sensitivity analysis for conductivity values

For a given model anatomy, the simulated recordings will depend on the tissue conductivities, the location of the bioelectric sources, and the positions of the recording contacts. In order to study the effects of conductivity variations, we first sought to fix the source locations and the positioning of the cuff electrode.

The source locations (i.e., the position of the neural pathways within the cross-section of the nerve) were selected based on the similarity of simulated recordings with the experimental data. The ith column of **L** is an 8x1 column vector giving the recordings that would be produced by a dipolar source in the ith mesh element. Another 8x1 vector **m** was formed using the peak values at each of the 8 contacts in the averaged experimentally recorded waveforms, for each stimulus type. The mesh element for which the absolute values of the corresponding column in **L** had the highest Pearson's correlation coefficient with **m** was used to define the position of the neural pathway in the model. This process was repeated for each of the three types of stimuli (designed to activate the tibial, peroneal and sural fascicles), resulting in three pathway locations. We hereafter use the notation $\mathbf{m}_f$ and $\mathbf{L}_f$ to refer to the experimental and simulated 8x1 vectors, respectively, with f = {tibial, peroneal, sural}. Only mesh elements located in the endoneurium were used for this analysis.

The values in **L** depend not only on the location of the bioelectric source, but also on the positioning of the recording contacts. Because the sciatic nerve was not exactly 1.00 mm in diameter and because the surrounding saline in the model had to have a minimum width for successful meshing, the final inner diameter of the nerve cuff electrode in the model was greater than 1 mm (inner diameter of 1.66 mm). The electrode spacing in the cuff is designed for an inner diameter of 1 mm, so if the nerve is larger the 8 contacts will not wrap completely around the nerve. However, the exact location of the contacts around the nerve is not known. To account for this, 14 electrode contacts were used instead of 8 in the FE model, which was the number of contacts required to wrap around the nerve while maintaining the correct electrode spacing. Then, every possible combination of 8 consecutive contacts was investigated (e.g., contacts 1-8, 2-9, …, 14-7). The pathway localization process described in the previous paragraph was repeated for each of these contact subsets. The subset that yielded the highest correlations between the

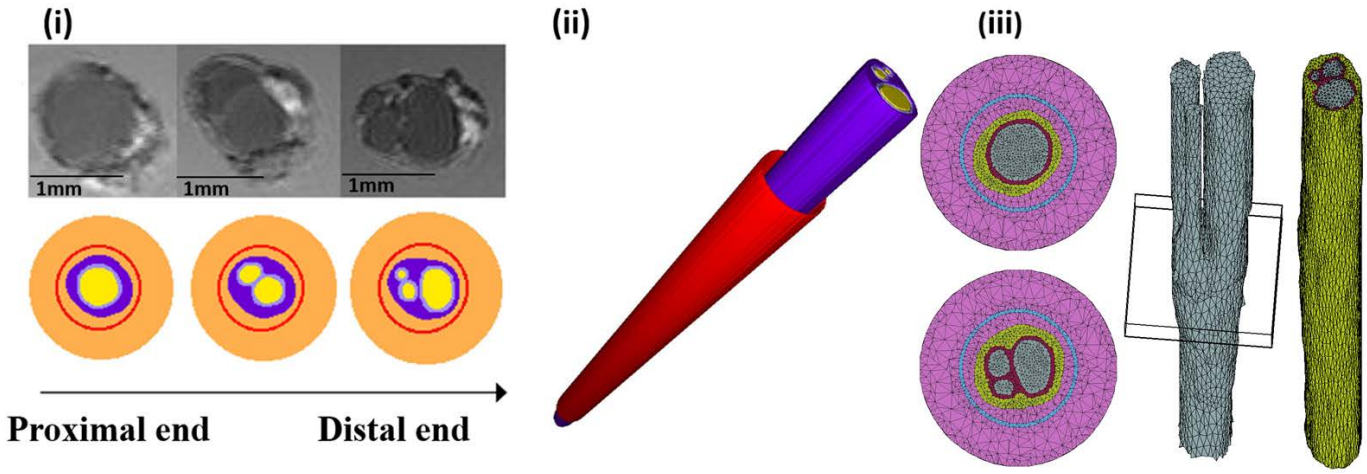

Fig. 4. (i) Segmentation of selected cross sections of the rat sciatic nerve from proximal to distal end. The fascicles bifurcate into tibial and peroneal fascicles, and then the tibial fascicle bifurcates into the sural fascicle. (ii) Volumetric isosurface of the nerve with the cuff electrode; (iii) Cross section of tetrahedral mesh at proximal end and at distal end; longitudinal changes in the mesh denoting the endoneurium tissue; tetrahedral mesh of the nerve(nerve cuff not shown). The frame around the endoneurium mesh denotes the region with z-coordinates in the range of 16 mm to 17 mm, which is the region from which the slices in Figure 5 are drawn.

simulated and experimental data was retained for the rest of the analysis.

Having fixed the location of the neural pathways and cuff contacts, we varied the conductivity values for the endoneurium, perineurium and epineurium tissue layers one at a time to investigate their effects on the simulation results. The endoneurium tissue layer is anisotropic in nature, varying radially and longitudinally, so we varied each of those conductivities individually. We varied the base values (as listed in Section II.B.4) by a defined step size. The new values were changed by a step size of ±10% of the base value, with 10 steps in each direction. For each set of conductivity values, we simulated the recordings by conducting a new FE analysis in SCIRun. Analysis of the results was performed in MATLAB.

Two metrics were used to quantify the results:

- The correlation coefficient between $\mathbf{L}_f$ and $\mathbf{m}_f$, as a function of the conductivity values. This measure quantifies how the variations in the conductivities affect the ability of the model to reproduce the experimental data, and therefore to produce realistic variations between the recordings at different contacts.
- The Selectivity Index (SI), which has been used in previous studies [12, 17]. We used the definitions found in [17], and reproduced here in Appendix. Briefly, the SI quantifies the difference in recording patterns obtained from two different pathways in the nerve. This distance measure was computed for all pairwise combinations of $\mathbf{L}_{tibial}$, $\mathbf{L}_{peroneal}$ and $\mathbf{L}_{sural}$, and we report the average of these values. The SI does not reflect how well the model can reproduce the experimental observations, but rather we used it to determine how incorrect conductivity estimates might affect conclusions about the selectivity of nerve cuff recordings.

D. Influence of anatomical detail on simulated recordings

The pathway and cuff contact positions determined using the methods described in Section II.C. were used for this portion of the analysis. Tissue conductivity values were set to the base values listed in Section II.B.4.

To generate simulated action potentials from the model constructed as described above, neural pathways for each fascicle were laid out. The process described in Section II.C. provided the location of one point for each pathway. Additional points were manually defined for each pathway at the distal and proximal ends of the nerve. A spline interpolation was then defined to create from these three points a pathway along the entire length of the nerve, for each fascicle. The positions of Nodes of Ranvier along these pathways were decided based on the fiber type. For our analysis, we used Aα fibers with a conduction velocity of 80 m/sec and a distance between Nodes of Ranvier of 1.65 mm. Only one type of fiber was used in these simulations in order to minimize the number of varying parameters, and focus on the influence of the anatomical structures.

The resulting model can be used to generate simulated recordings from the tibial, peroneal and sural fascicles. Using this model, our last step was to investigate the effect of the level of anatomical detail on the simulated recordings. Specifically, we sought to determine if there was value in modelling the progressive branching of the fascicles, in contrast to using a model whose cross-section remains constant for the entire length of the nerve, as has been the case to date in the literature. For this comparison, the nerve cuff design used in the model had 98 contacts organized in 7 rings of 14 contacts (See Section II.C.) spread along the length of the nerve. The length of the nerve cuff was the same as for the 8-channel cuffs used in the previous simulations (22 mm). The rationale for the additional rings of contacts in this portion of the analysis is to allow us to examine the effects of the anatomy on the recordings at different point along the fascicular branching. Thus, the anatomically accurate FE model was used to simulate the recordings of a 98-contact cuff electrode, and the results were compared with those obtained from a model with a lower level of anatomical accuracy. The simpler model was obtained by taking a single cross-section from the MRI data and extruding it to obtain a longitudinally uniform 3D model. For this model, the neural pathways were straight along the axis of the nerve. For each of the 98 contacts, the percentage difference in the peak values obtained from each of the two models was computed, after normalizing

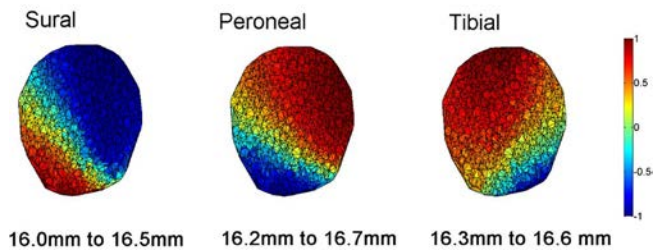

Fig. 5: Correlation coefficients between simulated and *in vivo* recordings for endoneurium elements in the given cross sections. The left figure refers to correlations with recordings from the sural fascicle, the middle figure to recordings from the peroneal fascicle, and the right figure to recordings from the tibial fascicle.

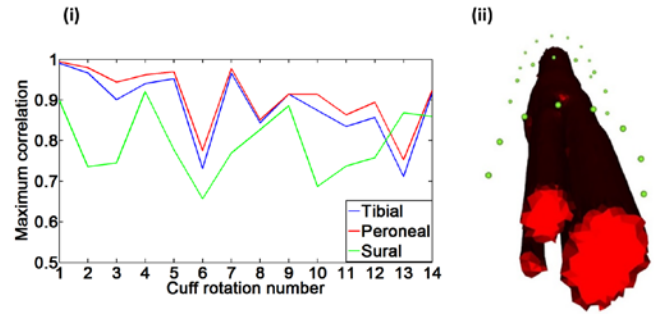

Fig. 6. (i) Correlation between *in vivo* data and simulated data of three fascicles using base conductivity values, as the cuff rotation is varied; (ii) Position of cuff electrode contacts onto the fascicles for Rotation 1.

the values in each model to a contact in the middle ring. This analysis will help determine whether the additional anatomical complexity is warranted or if simpler models can yield comparable results.

III. RESULTS

A. Neural recordings

Figure 2 shows an example of recordings obtained from the 8-channel nerve cuff. The average waveforms are shown in Figure 3, after aligning the detected APs to their positive peak. A total of 175 APs were used to obtain the dorsiflexion average waveform, while 207 APs were used for the plantarflexion waveform and 231 APs for the heel prick waveform.

B. FE Model Construction

The MRI scan of the sciatic nerve consisted of 86 slices with a thickness of 250 μm. The total FE nerve length was 26mm (the most proximal and most distal slices were duplicated to extend the model to the desired length). The fascicles were segmented manually in each slice, with the proximal end of the nerve having one fascicle which divided into three fascicles towards the distal end. The modeling steps are illustrated in Figure 4. Note that the center ring of the nerve cuff, containing the 8 recording contacts, was positioned slightly proximally to the branching of the fascicles. For the investigation of the influence of the anatomical detail (see Section II.D.), a second tetrahedral mesh was computed with uniform anatomy in the longitudinal direction. The cross-section shown in Figure 4(i) (distal end) was used for this purpose. A slice was chosen slightly distal to the branching of the fascicles, and extruded longitudinally to obtain the 3D model. In this way, the simplified model included distinct fascicles and a realistic cross-sectional anatomy, but with no branching.

C. Influence of tissue conductivities

As described in Section II.C., studying the effects of changes in tissue conductivities first required fixing the positioning of the neural sources and electrode contacts. Figure 5 shows examples of how the correlation between $\mathbf{L}_f$ and $\mathbf{m}_f$ varied as a function of the mesh element in which the dipolar source was placed, for a few selected slices of the model. Only elements within certain sub-sections of the nerve model produced simulated signals that correlate well with the *in vivo* recordings. This figure thus supports the notion that the position of the source is an important parameter to consider.

As for the cuff rotation, Figure 6(i) shows how the maximum correlation found between $\mathbf{L}_f$ and $\mathbf{m}_f$ varied when different subsets of contacts were used. Based on these results, we selected Rotation 1 for the remainder of this analysis (maximum correlation close to 1 for the tibial and peroneal fascicles, and second highest correlation for the sural fascicle with 0.89). The positions of the contacts in this subset are shown in Figure 6(ii).

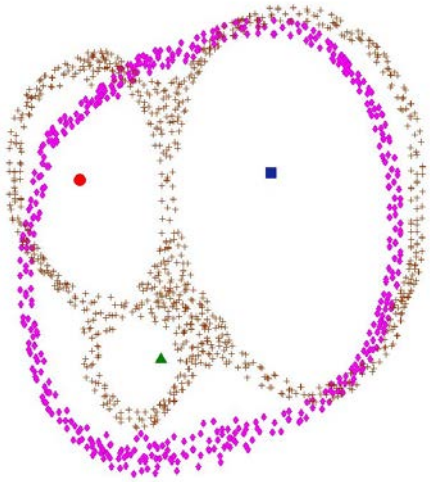

Fig. 7: Identified pathway locations within the nerve cross-section, using the base conductivity values. The pink boundary shows the central slice where the recording contacts were placed, whereas, the brown boundary shows the boundary of the perineurium from a slightly more distal slice where the fascicles had branched. The more distal slice is shown here for reference to evaluate the realism of the pathway placements. The blue square box shows the element with maximum correlation with peroneal recordings, whereas the red dot corresponds to the tibial recordings and the green triangle to the sural recordings.

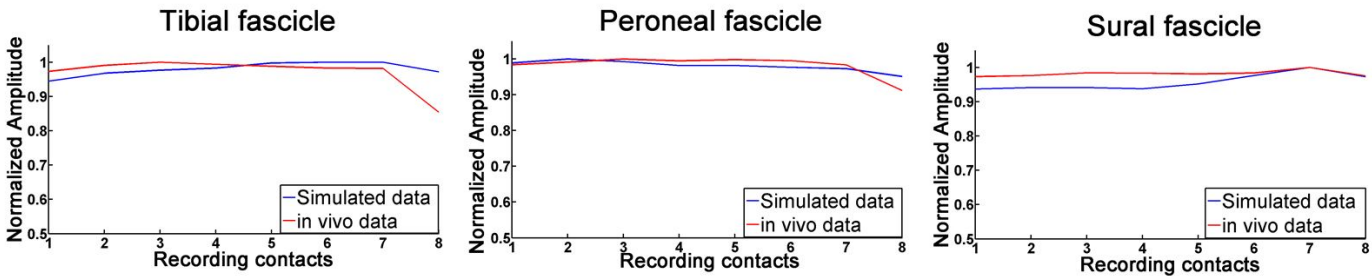

Fig. 8. Comparison of simulated and *in vivo* neural recordings for tibial, peroneal and sural fascicles.

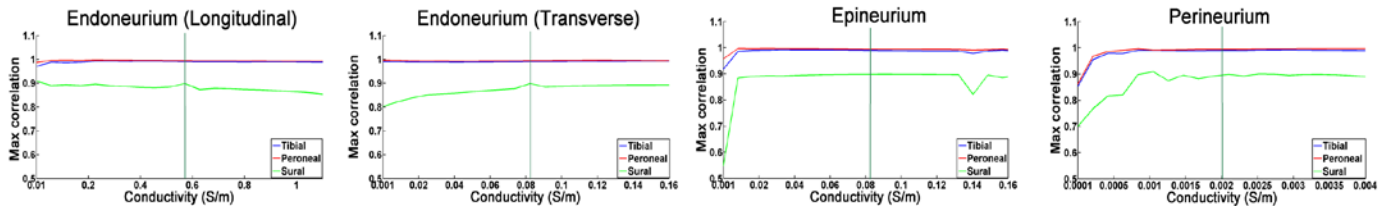

Fig. 9: Changes in the correlation between the simulated and experimental neural recordings, as a function of the tissue conductivity values. Vertical bars denote the base conductivities.

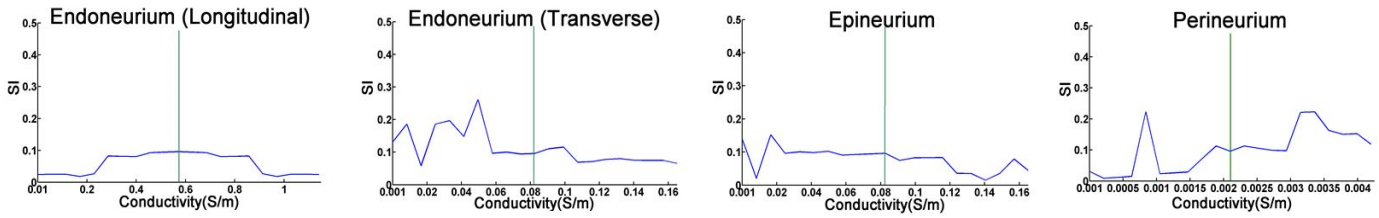

Fig. 10. Changes in SI, as a function of the tissue conductivity values. Vertical bars denote the base conductivities.

With these contact positions, the neural source locations that maximized the correlation between $\mathbf{L}_f$ and $\mathbf{m}_f$ for each of the stimulus types are shown in Figure 7. Note that Figure 7 is a 2-dimensional projection onto the x-y plane (cross-section of the nerve). Not all of the identified mesh elements were at the same position along the z-axis (longitudinal direction along the nerve). However, all three of them were within 1.82±0.12 mm of the position of the middle ring of the cuff along the z-axis. By comparing these locations with a distal slice where the fascicles had branched, we found that the pathway locations were consistent with expected anatomy. $\mathbf{m}_f$ was then compared with the selected $\mathbf{L}_f$ for each fascicle (Figure 8). For this comparison, the peak values were normalized to the maximum value across the 8 contacts. It was seen that the simulated and experimental recording patterns were similar for all fascicles, although some deviation could be observed in the tibial fascicle. Nonetheless, the *in vivo* recordings appear to validate our simulation results. All of the steps above were conducted using the base conductivity values.

With the source and contact positions fixed, Figure 9 shows how the correlation between $\mathbf{L}_f$ and $\mathbf{m}_f$ varied as a function of each tissue conductivity. High correlations for the tibial and peroneal fascicles (0.97) and slightly lower correlation for the sural fascicle (0.89) were found across a broad range of conductivity values.

These correlation values are only sensitive to the patterns, not amplitudes, of the signals compared. Conductivity changes are expected to affect signal amplitudes. Therefore, to use a selectivity metric more sensitive to amplitudes, we examined how the SI changes as a function of the conductivity values (Figure 10). This analysis confirmed that the SI is more sensitive to the changes in conductivities than the correlation metric used above, but relatively small variations around the base conductivity values still did not have a substantial impact on the results (with the exception of a decrease in perineurium conductivity, which led to a trend toward decreased selectivity). These results support the notion that the conductivity variations affect the amplitudes of the simulated recordings more than the patterns of activation across contacts.

D. Influence of anatomical detail

Based on the analysis above, we chose parameter values for the final FE model. The pathway locations and cuff positioning were determined as described in Section III.C. The results in Figures 9 and 10 showed that varying the conductivities will have a minimal effect on any conclusions regarding nerve cuff recording selectivity. Therefore, we have opted to keep using the base conductivity values as found in the literature and listed in Section II.B.4, because our simulations do not provide strong evidence in favour of using any different values.

Having thus finalized the model, we sought to check the importance of the added anatomical detail in our model. We compared the recordings obtained from the detailed and simplified models (see Section III.B.), when using a multicontact electrode with 7 rings of 14 contacts. Figure 11 shows how the electrode contacts were placed with respect to the endoneurium in each model. The increase in the number of

Fig. 11: Position of the seven rings of recording contacts with respect to the endoneurium, in the anatomically detailed model (left) and simplified model (right).

contacts in the cuff electrode for this analysis was intended to better capture longitudinal variations in the recordings, as the fascicles branch at the distal end. The neural pathways that were defined for the detailed model, as discussed in Section II.D., are shown in Figure 12.

The pattern of peak values of these APs across all 98 contacts was then compared between the two models (Figure 13). These values are normalized to one contact in the middle ring. The mean difference in amplitude with respect to the simplified model was 30.20% ± 21.81, 22.03% ± 12.92 and 99.46% ± 77.46 in the tibial, peroneal and sural fascicles respectively (mean and standard deviation values reported over the 98 contacts).

IV. DISCUSSION

In order to design improved peripheral nerve interfaces, FE models have been used on multiple occasions to simulate neural recordings [16-20]. In this study, we focused on two modeling decisions that are ubiquitous in the literature to date, but have never been explicitly evaluated: the conductivities of the neural tissues, and the use of a simplified anatomy. To this end, we constructed a novel FE peripheral nerve model that is the first to reflect the progressive branching of the fascicles, and the first to be validated directly using electrophysiological recordings.

A. Construction of the FE model

The FE model of the sciatic nerve was constructed using MRI volumetric images. Possible sources of inaccuracy in this process include manual image segmentation, the limited resolution of the images (30μm x 30 μm x 250 μm), and the excess width of the perineurium and saline layers due to meshing constraints. While it is possible that these factors may have affected our results to some degree, the model developed here is still considerably closer to the nerve's true anatomy than any previously reported model. Furthermore, the fact that the model was able to reproduce the *in vivo* recordings using pathway locations that were fully consistent with the expected anatomy (Figure 7) is a strong argument for its validity.

B. Tissue conductivities

We found that variations in the conductivity values did not have a substantial impact on the ability of the model to reproduce the patterns of inter-contact variations observed *in vivo*. On the other hand, since the conductivities determine the amplitudes of the recorded signals (as partially reflected by our results for the SI), they could reduce selectivity through alterations to the SNR. What our results suggest is that in any simulation study in which noise is added to the recordings using a predefined SNR, changes to the conductivity values would not alter conclusions about recording selectivity to any significant degree. Importantly, our analysis is not intended to provide evidence for or against the accuracy of the conductivity values used to date; rather, our objective was to determine to what extent errors in these values could be leading to erroneous conclusions.

Irregularities were observed in the SI estimates as the conductivity values decreased away from the default values. A possible reason for this trend is that the $\mathbf{L}_f$ patterns obtained for each of the three fascicles do not always vary at the same speed with the changes in conductivity, as reflected in Figure 9. If, at a given conductivity value, there is a greater change in one fascicle than the others, this divergence may be reflected in the SI. For example, the sudden peak in the perineurium SI plot between 0.0005 and 0.001 S/m (Figure 10) corresponds to a point in Figure 9 where the sural correlation drops before the tibial and peroneal correlations do.

C. Anatomical detail

We sought to determine the degree to which the added level of anatomical detail altered the simulation results. We simulated the neural recordings using a nerve cuff electrode with seven rings of contacts, in both the anatomically detailed model and in a longitudinally uniform model based on a single detailed cross-section. Increasing the number of rings provided information about recordings at the proximal end of the endoneurium, where the fascicle has no branching in the anatomically accurate model, as well as the distal end, where there are three individual fascicles. The results suggest that incorporating the progressive branching of the fascicles into the model has a large impact on the simulation results (50.56% ± 37.40% change in amplitudes, across the 98 simulated contacts). In Figure 13, we can see that the differences are highest between recording contacts 1 to 38. In this range, the recordings were taken from the unifascicular endoneurium in case of the branching model, whereas the simplified model remains constant with three fascicles longitudinally. The observed differences are therefore consistent with the

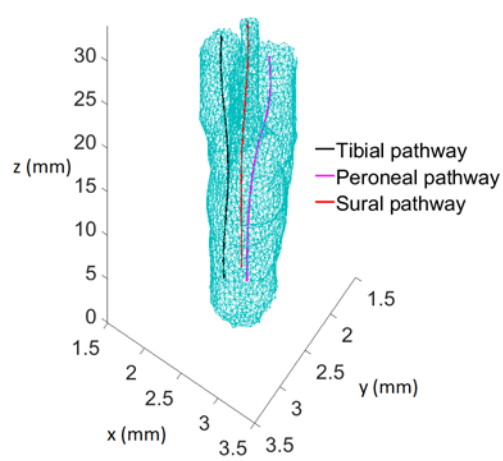

Fig. 12. Pathways of tibial, peroneal and sural fascicle along the anatomically accurate FE model.

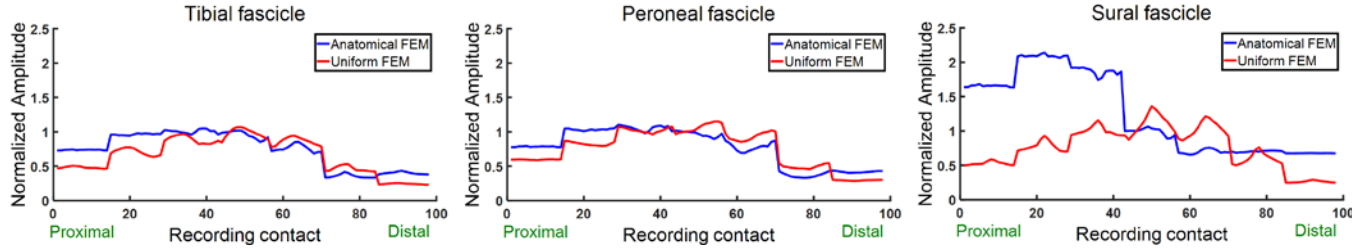

Fig. 13. Normalized recording patterns of the anatomically detailed model and simplified model in all rings for the sural, peroneal and tibial fascicles.

underlying anatomy of the two models, at least in the case of the tibial and peroneal fascicles. The sural fascicles exhibited larger differences. While we cannot conclusively state the reason for this, the sural fascicle is smaller than the other two. In the simplified model, this small fascicle runs the whole length of the nerve; in contrast, in the more detailed model, the small fascicle at the distal end merges into the larger unifascicular trunk at the proximal end, which could have affected the amplitude of the recordings obtained. As expected, the differences between the models were most pronounced at the proximal end of the nerve, where the anatomies were most different (unifascicular vs. multifascicular). Branching models are therefore likely to be of importance primarily in electrode designs that include contacts at multiple sites along the length of the nerve, which has previously been shown to be beneficial [21].

D. *Limitations*

In the *in vivo* recordings, the signal variations between contacts were small, and relatively similar for the three fascicles, in particular the tibial and peroneal fascicles (Figure 8). Therefore, all of the correlations between the simulated and experimental data had to rely on analyzing small variations. We have attempted to mitigate this limitation through the use of average waveforms obtained from a large numbers of APs. Nonetheless, it is possible that our results may have been more robust or informative if there had been more variability in the *in vivo* recordings to guide the modeling.

Importantly, the model parameters were validated only for simulating *in vivo* recordings. The model was not validated for its ability to predict the effects of nerve stimulation. For example, it is expected that the conductivity values would prove to be more important in that context. Our focus here was on creating a tool to simulate multi-contact nerve cuff recordings and guide the development of electrodes capable of more selective recordings. Future work could focus on determining how our new model can be beneficial for the development of neural stimulation applications.

V. CONCLUSION

We have developed and validated a realistic peripheral nerve model that can be used for quantitatively accurate simulations of nerve cuff recordings. This model was used here to examine the effects of two common modeling decisions found in previously reported work. The simulation results were found not to be very sensitive to conductivity variations, but the added anatomical detail considerably altered the results, suggesting that this a factor that should be considered more carefully in future modelling studies. Going forward, we have created a simulation tool that may be used in the development of improved neural interfaces.

VI. ACKNOWLEDGMENTS

The authors gratefully acknowledge the assistance of Dr. Warren Foltz for the MRI imaging, and Tianyu Zhou for the processing of the recordings.

VII. APPENDIX

The equations used for the SI were obtained from [17] and are reproduced here. Considering a case with N contacts and M fascicles, let V_i be the vector for fascicle *i*, consisting of N elements v_{ij} that correspond to the value recorded at contact *j* when fascicle *i* is active. Each V_i is normalized as shown in Eq. 1 to eliminate the effect of contact impedance.

$$c_{ij} = \frac{v_{ij}}{\sum_{k=1}^{M} v_{kj}} \tag{1}$$

The vector for each fascicle is then normalized to unit magnitude (Eq. 2):

$$Wi = (w_{i1}, w_{i2}, \dots, w_{iN}) \tag{2}$$

Where:

$$w_{ij} = \frac{c_{ij}}{\sqrt{c_{i1}^2 + c_{i2}^2 + \cdots + c_{iN}^2}} \tag{3}$$

The distance measure between two fascicles is then computed as shown in Eq. 4.

$$SI(W_i, W_k) = \frac{\sqrt{(w_{i,1} - w_{k,1})^2 + \cdots + (w_{i,N} - w_{k,N})^2}}{\sqrt{2}} \tag{4}$$

In this work, the final SI obtained by taking the average of the pairwise comparisons between the three fascicles.

VIII. REFERENCES

[1] P. H. Peckham and J. S. Knutson, "Functional electrical stimulation for neuromuscular applications," *Annu. Rev. Biomed. Eng.*, vol. 7, pp. 327-360, 2005.

[2] J. del Valle and X. Navarro, "Interfaces with the peripheral nerve for the control of neuroprostheses," *Int. Rev. Neurobiol.*, vol. 109, pp. 63-83, 2013.

[3] J. Ordonez, M. Schuettler, C. Boehler, T. Boretius and T. Stieglitz, "Thin films and microelectrode arrays for neuroprosthetics," *MRS Bull*, vol. 37, pp. 590-598, 2012.

[4] R. B. Stein, T. R. Nichols, J. Jhamandas, L. Davis and D. Charles, "Stable long-term recordings from cat peripheral nerves," *Brain Res.*, vol. 128, pp. 21-38, 1977.

[5] D. B. Popovic, R. B. Stein, K. L. Jovanovic, R. Dai, A. Kostov and W. W. Armstrong, "Sensory nerve recording for closed-loop control to restore motor functions," *Biomedical Engineering, IEEE Transactions On*, vol. 40, pp. 1024-1031, 1993.
[6] J. J. Struijk, M. Thomsen, J. O. Larsen and T. Sinkjaer, "Cuff electrodes for long-term recording of natural sensory information," *IEEE Eng. Med. Biol. Mag.*, vol. 18, pp. 91-98, 1999.
[7] M. K. Haugland and T. Sinkjaer, "Cutaneous whole nerve recordings used for correction of footdrop in hemiplegic man," *IEEE Trans. Rehab. Eng.*, vol. 3, pp. 307-317, 1995.
[8] F. J. Rodriguez, D. Ceballos, M. Schuttler, A. Valero, E. Valderrama, T. Stieglitz and X. Navarro, "Polyimide cuff electrodes for peripheral nerve stimulation," *J. Neurosci. Methods*, vol. 98, pp. 105-118, June 1, 2000.
[9] B. K. Lichtenberg and C. J. De Luca, "Distinguishability of functionally distinct evoked neuroelectric signals on the surface of a nerve," *IEEE Trans. Biomed. Eng.*, vol. 26, pp. 228-237, April, 1979.
[10] J. J. Struijk, M. K. Haugland and M. Thomsen, "Fascicle selective recording with a nerve cuff electrode," in *Proceedings of the 18th Annual International Conference of the IEEE Engineering in Medicine and Biology Society*, 1996, pp. 361-362.
[11] P. R. Christensen, Y. Chen, K. D. Strange, K. Yoshida and J. A. Hoffer, "Multi-channel recordings from peripheral nerves: 4. evaluation of selectivity using mechanical stimulation of individual digits." in *Proc. 2nd Ann. Conf. IFESS*, 1997, .
[12] P. B. Yoo and D. M. Durand, "Selective recording of the canine hypoglossal nerve using a multicontact flat interface nerve electrode," *IEEE Trans. Biomed. Eng.*, vol. 52, pp. 1461-1469, August, 2005.
[13] B. Wodlinger and D. M. Durand, "Selective recovery of fascicular activity in peripheral nerves," *J. Neural Eng.*, vol. 8, pp. 056005, October, 2011.
[14] J. Zariffa, M. K. Nagai, M. Schuettler, T. Stieglitz, Z. J. Daskalakis and M. R. Popovic. Use of an experimentally derived leadfield in the peripheral nerve pathway discrimination problem. *IEEE Transactions on Neural Systems and Rehabilitation Engineering*, 19(2), pp. 147-56. 2011.
[15] D. T. Plachta, M. Gierthmuehlen, O. Cota, N. Espinosa, F. Boeser, T. C. Herrera, T. Stieglitz and J. Zentner, "Blood pressure control with selective vagal nerve stimulation and minimal side effects," *Journal of Neural Engineering*, vol. 11, pp. 036011, 2014.
[16] J. H. Meier, W. L. C. Rutten and H. B. K. Boom, "Extracellular potentials from active myelinated fibers inside insulated and noninsulated peripheral nerve," *IEEE Trans. Biomed. Eng.*, vol. 45, pp. 1146-1154, 1998.
[17] J. Perez-Orive and D. M. Durand, "Modeling study of peripheral nerve recording selectivity," *IEEE Trans. Rehabil. Eng.*, vol. 8, pp. 320-329, September, 2000.
[18] A. Q. Choi, J. K. Cavanaugh and D. M. Durand, "Selectivity of multiple-contact nerve cuff electrodes: a simulation analysis," *IEEE Trans. Biomed. Eng.*, vol. 48, pp. 165-172, February, 2001.
[19] J. Zariffa and M. R. Popovic. Localization of active pathways in peripheral nerves: A simulation study. *IEEE Transactions on Neural Systems and Rehabilitation Engineering*, 17(1), pp. 53-62. 2009.
[20] B. Wodlinger and D. M. Durand, "Localization and recovery of peripheral neural sources with beamforming algorithms," *IEEE Trans. Neural Syst. Rehabil. Eng.*, vol. 17, pp. 461-468, October, 2009.
[21] J. Zariffa, M. K. Nagai, Z. J. Daskalakis and M. R. Popovic. Influence of the number and location of recording contacts on the selectivity of a nerve cuff electrode. *IEEE Transactions on Neural Systems and Rehabilitation Engineering*, 17(5), pp. 420-7. 2009.
[22] M. Gierthmuehlen, T. M. Freiman, K. Haastert-Talini, A. Mueller, J. Kaminsky, T. Stieglitz and D. T. Plachta, "Computational tissue volume reconstruction of a peripheral nerve using high-resolution light-microscopy and reconstruct," *PloS One*, vol. 8, pp. e66191, 2013.
[23] J. B. Ranck and S. L. BeMent, "The specific impedance of the dorsal columns of cat: an anisotropic medium," *Exp. Neurol.*, vol. 11, pp. 451-463, 1965.
[24] A. Weerasuriya, R. A. Spangler, S. I. Rapoport and R. E. Taylor, "AC impedance of the perineurium of the frog sciatic nerve." *Biophys. J.*, vol. 46, pp. 167, 1984.
[25] T. Stieglitz, H. Beutel, M. Schuettler and J. W. Meyer, "Micromachined, polyimide-based devices for flexible neural interfaces," *Biomed. Microdevices*, vol. 2, pp. 283-294, 2000.
[26] R. R. Riso, F. K. Mosallaie, W. Jensen and T. Sinkjaer, "Nerve cuff recordings of muscle afferent activity from tibial and peroneal nerves in rabbit during passive ankle motion," *IEEE Trans. Rehabil. Eng.*, vol. 8, pp. 244-258, June, 2000.
[27] R. W. Clarke, S. Eves, J. Harris, J. E. Peachey and E. Stuart, "Interactions between cutaneous afferent inputs to a withdrawal reflex in the decerebrated rabbit and their control by descending and segmental systems," *Neuroscience*, vol. 112, pp. 555-571, 2002.
[28] W. S. Rasband, "ImageJ, US National Institutes of Health, Bethesda, Maryland, USA, h ttp," *Imagej.Nih.Gov/Ij*, vol. 2012, 1997.
[29] Center for Integrative Biomedical Computing, "Seg3D: Volumetric Image Segmentation and Visualization. Scientific Computing and Imaging Institute (SCI)," 2015.
[30] Q. Fang and D. A. Boas, "ISO2Mesh: a 3D surface and volumetric mesh generator for matlab/octave," 2010.
[31] D. Weinstein, L. Zhukov and C. Johnson, "Lead-field bases for electroencephalography source imaging," *Annals Biomed. Eng.*, vol. 28, pp. 1059-1065, 2000.
[32] Scientific Computing and Imaging Institute, (SCI), "SCIRun: A Scientific Computing Problem Solving Environment," 2015.

Purbasha Garai was born in West Bengal, India, in 1992. She received the B.tech degree in biomedical engineering from the Vellore Institute of Technology, Vellore, India and the M.A.Sc degree in Biomedical Engineering from the University of Toronto, Toronto, Canada.

From 2013 to 2016, she was a graduate student researcher with the Adaptive Neurorehabilitation Systems Lab under the supervision of Dr. José Zariffa. Her research interests include finite element modeling, peripheral nerve interfaces, nerve imaging and nerve cuff recordings.

Ms. Garai was a recipient of the Dean's merit scholarship at the Vellore Institute of Technology in 2011 and an entrance scholarship at the University of Toronto.

Ryan G. L. Koh (SM'16) is a Ph.D. candidate at the Institute of Biomaterials and Biomedical Engineering, University of Toronto, Toronto, Ontario, Canada. He previously received a B.Eng. in Electrical and Biomedical engineering at McMaster University

He is interested in the field of rehabilitation engineering, with specific areas of interest in peripheral nerve recordings and functional electrical stimulation therapy. Currently, he is working on developing algorithms to improve the selectivity of peripheral nerve recordings at the Toronto Rehabilitation Institute – University Health Network.

Martin Schuettler (M'99) studied electrical engineering at the Technical University of Braunschweig, Germany, and received his PhD on peripheral nerve stimulation electrodes from Saarland University, Germany, in 2002.

From 2003 to 2005 he joined the Implanted Devices Group at University College London, U.K., as post-doctoral fellow, working on strategies of selective peripheral nerve recordings. Dr. Schuettler had several extended visits to the Australian Visual

Prosthese Group. Since 2005 he became group leader at the Laboratory for Biomedical Microtechnology at the University of Freiburg, Germany. In 2010, he co-founded CorTec, a spin-off company developing and commercializing human implantable brain-machine interfaces. Since 2015 he holds the position of CEO/CTO at CorTec.

Dr Schuettler has published more than 150 peer-reviewed papers, abstracts and book chapters.

Thomas Stieglitz (M'95–SM'09) received a Diploma degree in electrical Engineering from Technische Hochschule Karlsruhe, Germany, in 1993, and a PhD and habilitation degree in 1998 and 2003 from the University of Saarland, Germany, respectively. In 1993, he joined the Fraunhofer Institute for Biomedical Engineering in St. Ingbert, Germany, where he established the Neural Prosthetics Group. Since 2004, he is a full professor for Biomedical Microtechnology at the Albert-Ludwig-University Freiburg, Germany, in the Department of Microsystems Engineering (IMTEK) at the Faculty of Engineering. His research interests include neural interfaces and implants, biocompatible assembling and packaging and brain machine interfaces.

Dr. Stieglitz has co-authored about 100 peer reviewed journal publications, 300 conference proceedings and holds 18 patents. He is co-founder and scientific consultant of CorTec GmbH and neuroloop GmbH, two spin-off companies which focus on neural implant technology and neuromodulation, respectively. Dr. Stieglitz is member of the IEEE EMBS, the Materials Research Society, the German Biomedical Engineering Society (DGBMT im VDE) where he is chair of the Neural Prostheses and Intelligent Implants section and founding member of the International Functional Electrical Stimulation Society (IFESS).

José Zariffa (M'01) received the Ph.D. degree in 2009 from the University of Toronto's Department of Electrical and Computer Engineering and the Institute of Biomaterials and Biomedical Engineering. He later completed post-doctoral fellowships at the International Collaboration On Repair Discoveries (ICORD) at the University of British Columbia in Vancouver, Canada, and at the Toronto Rehabilitation Institute – University Health Network in Toronto, Canada.

He is a currently a Scientist at the Toronto Rehabilitation Institute – University Health Network and an Assistant Professor at the Institute of Biomaterials and Biomedical Engineering at the University of Toronto in Toronto, Canada. His research interests include technology for upper limb rehabilitation after spinal cord injury, neural prostheses, and interfaces with the peripheral nervous system.

Dr. Zariffa was awarded the 1st place award (Research Category) at the 2012 National Spinal Cord Injury Conference for his work on the motor control of the upper limb after spinal cord injury.